Volume 1 | Number 1 | Jan 2013 | Pages 1–100

Nanoscale

www.rsc.org/nanoscale

ROYAL SOCIETY OF CHEMISTRY

ROYAL SOCIETY OF CHEMISTRY

www.rsc.org/nanoscale

Nanoscale

ARTICLE

Synthesis of Vinyl-Terminated Au Nanoprisms and Nanooctahedra Mediated by 3-Butenoic Acid: Direct Au@pNIPAM Fabrication with Improved SERS Capabilities

M. A. Casado-Rodriguez,[a] M. Sanchez-Molina[a], A. Lucena-Serrano,[c] C. Lucena-Serrano,[a] B. Rodriguez-Gonalez,[b] Manuel Algarra,[c] Amelia Diaz,[a] M. Valpuesta,[a] J. M. Lopez-Romero,[a] J. Perez-Juste,[b*] R. Contreras-Caceres.[a*]

Here we describe the first seedless synthesis of vinyl-terminated Au nanotriangular prisms (AuNTPs) and nanooctahedra (AuNOC) in aqueous media. This synthesis is performed by chemical reduction of chloroauric acid ($HAuCl_4$) with 3-butenoic acid (3BA) in presence of benzyldimethylammonium chloride (BDAC). The principal novelties of the presented method are the use of a mixture of 3BA and BDAC, the synthesis of gold prisms and octahedra with controllable size, and the presence of terminal double bonds on the metal surface. Initially this method produces a mixture of triangular gold nanoprisms and octahedra, however, both morphologies are successfully separated by surfactant micelle induced depletion interaction, reaching percentages up to ~90 %. Moreover, the alkene moieties presented on the gold surface are exploited for the fabrication of hybrid core@shell particles. Gold octahedra and triangular prisms are easily encapsulated by free radical polymerization of *N*-isopropylacrylamide (NIPAM). Finally, in order to obtain a gold core with the most number of tips, AuNTP@pNIPAM microgels were subjected to gold core overgrowth, thus resulting in star-shaped nanoparticles (AuSTs@pNIPAM). We use 4-aminobenzenethiol as model analyte for SERS investigations. As expected, gold cores with tips and high curvature sites produced the highest plasmonic responses.

1. Introduction

Nowadays, the interest in the fabrication of noble metal nanoparticles with a great variety of sizes and morphologies is motivated by the advances in the understanding of their synthesis and properties,[1,2] as well as the possibility of being applied in a vast number of fields such as drug delivery,[3,4] DNA analysis,[5,6] cancer diagnosis[8] and treatment,[9,10] immunoassay,[7] and SERS and catalytic investigations.[11,12]

The properties of noble metal nanoparticles arise from the localized surface plasmon resonance (LSPR),[13,14] which remarkably depends, among other factors, on particle size and shape.[13,15] Since the first synthesis concerning gold nanoparticles only produced spherical shapes,[16] important efforts have been performed in the development of synthetic routes for the fabrication of non-spherical morphologies. This interest in the synthesis of anisotropic metal nanoparticles is because morphologies containing well-defined

angles or tips possess a more localized plasmons, thus supplying further promising and attractive applications in the aforementioned fields.[17, 18]

During the last decades, several protocols regarding the synthesis of particles with different morphologies as triangles, rods, wires, octahedra, decahedra, cages or stars have been reported in water or organic media.[19-25] Colloidal suspensions of Au nanoparticles are typically prepared by reaction of a gold salt with a reducing agent, in presence of stabilizing "capping" molecules, which play an important role in controlling the nanoparticle morphology.[22,26-31] Concerning the fabrication of Au octahedra and triangular prisms, which are the morphologies fabricated in this work, several protocols have been reported. For instance, Xia et al. reported the synthesis of gold octhaedra by reducing $HAuCl_4$ with N-vinyl pyrrolidone in an aqueous solution in the presence of cetyltrimethylammonium chloride (CTAC).[21] Mirkin et al. fabricated gold octahedral, in high yield, via the controlled overgrowth of preformed seeds by Ag+-assisted, seed-mediated synthesis.[27] Liz-Marzán et al. obtained Au nanotriangles by using CTAC-capped gold nanoparticles as seeds, in presence of small amount of iodide ions, and using ascorbic acid as reducing agent.[32] More recently, a seedless approach to synthesize monodisperse Au nanotriangles in high yield (>90%) has been reported by Zhang et al.[33] Unfortunately, all these methods give rise to particles solely stabilized by surfactants, that is, with no other functional groups on

a. *Departamento de Química Orgánica, Facultad de Ciencias, Universidad de Málaga, 29071, Málaga, Spain*
b. *Departamento de Química Física, CINBIO, Universidade de Vigo and IBIV, 36310 Vigo, Spain*
c. *Departamento de Quimica Inorgánica, Facultad de Ciencias, Universidad de Malaga, 29071, Málaga, Spain*

the metal surface, that could be readily available to be used in further chemical reactions.

Nowadays, a lot of research effort is devoted to the synthesis of nanocomposite materials with a core-shell architecture. Such hybrid systems are typically composed by a metal core encapsulated within a polymer shell.[34] These nanocomposite materials have been demonstrated to display a better performance for sensing and catalytic purposes compared with pure metal nanoparticles.[34-37] They could also incorporate multiple functionalities and improve their colloidal stability.[38-41] However, to obtain such core-shell morphology a surface modification step of the nanoparticles surface is generally required. Recently, butenoic acid has been used as reducing agent for the synthesis of spherical and octahedral Au nanoparticles.[42,43] Additionally, this molecule incorporates terminal double bonds on the particle surface, which was exploited for the fabrication of core@shellAu@pNIPAM hybrid nanocomposites systems.[38,42]

Herein, we report a water-based seedless method for the synthesis of vinyl-terminated triangular Au nanoprisms and nanooctahedra with controllable size, with 3-butenoic acid acting as reducing, as well as, shape inducing agent. Initially, two main morphologies were obtained; triangular prisms (AuNTPs) and octahedra (AuNOCs). We analyze the influence of the temperature and gold salt concentration in the reaction mixture on the shape and the size of the particles. Both morphologies were successfully separated by surfactant micelle induced depletion interaction.[44,45] Additionally, the presence of terminal double bond on the Au nanoparticles surface (coming from 3BA) was exploited for the fabrication of core@shell hybrid systems by free radical polymerization of N-isopropylacrylamide (NIPAM); including octahedra, prisms and star-like (AuSTs@pNIPAM) gold cores. Finally, the SERS enhancement capabilities of the different core-shell hybrids was studied using 4-aminobenzenethiol (4ABT) as model analyte.

2. Experimental

2.1 Materials

3-Butenoic acid (3BA, 97%), cetyltrimethylammonium chloride (CTAC, ≥98%), benzyldimethylhexadecylammonium chloride (BDAC, ≥97%) and *N*-isopropylacrylamide (NIPAM, 97%) and 4-aminobenzenethiol (4ABT, 97%) were supplied by Aldrich. $HAuCl_4 \cdot 3H_2O$ (≥99.9% trace metal basis) was supplied by Sigma. *N,N'*-methylenebisacrylamide (BIS, ≥99.5%) was supplied by Fluka. 2,2'-Azobis(2-methylpropionamidine) dihydrochloride (AAPH, 97%) was supplied by Acros Organics. All reactants were used without further purification. Water was purified using a Milli-Q system (Millipore).

2.2 Characterization Methods

UV–vis measurements of aqueous colloidal solutions were recorded with a HP Agilent 8453 diode array spectrophotometer. Transmission electron microscopy (TEM) images were acquired on a JEOL JEM 1400 operating at an acceleration voltage of 80 kV. Samples were prepared by drying a 10 µL drop of colloidal suspension on a carbon-coated copper grid. HR-TEM images were acquired with a JEOL JEM2010F field-emission gun transmission

electron microscope, working at 200 kV. For this specific analysis, samples were prepared letting dry a drop of sample on TEM copper grids coated with holey carbon thin film. Field emission scanning electron microscopy (FESEM) images were obtained in a Helios Nanolab 650 Dual Beam from FEI, working at acceleration voltage of 15kV, a current intensity of 0.2 nA and a tilting angle of 52°. Sample were prepared by dropping 20 µL of an aqueous colloidal solution onto a 1x1 cm single side polished boron-doped silicon (111) wafer (WRS Materials). SERS spectra were measured using a confocal Raman Microscope (CRM) alpha300R, (WITec GmbH, Ulm, Germany). SERS signals were recorded by exciting the colloidal solutions with a laser power of 5 mW using a 785 nm laser line. For one Raman spectrum, between 50 and 200 single Raman spectra with a measuring time of 0.5s were accumulated. Raman spectra were recorded within the spectral range of 0-2500 cm^{-1} for Raman shift. Samples for SERS were prepared by adding 15 µL of 4ABT 10^{-3} mM to 1.5 mL of each sample (AuNOC@pNIPAM, AuNTPs@pNIPAM, AuSTs@pNIPAM, at a gold concentratio of 0.5 mM). After 1 h, allowing for thermodynamic equilibrium to be reached, the colloidal solution was centrifugated twice, and redispersed in 1.5 mL of water.SERS was directly recorded from these suspensions.

2.3 Synthesis of Au nanoparticles

In a typical synthesis, 50 mL of a solution containing 0.5 mM $HAuCl_4$ and 5 mM BDAC were introduced into a 100 mL round bottom flask under low magnetic stirring (100 rpm). Subsequently, the solution was heated up to 75°C, 85°C or 95°C. Then, 100µL of 3BA were added into the mixture. After a suitable amount of time enough to allow the complete reduction of $HAuCl_4$ to Au(0) (see Table 1) the solution was allowed to cool down at room temperature. Finally, in order to remove the excess of 3BA and BDAC, the colloidal dispersion containing the Au nanoparticles were centrifuged at 7500 rpm during 30 min. The supernatant was discarded and the pellet was dispersed in 50 mL of 4mM CTAC. The same procedure was followed for the synthesis at 1 mM and 1.5 mM $HAuCl_4$, keeping constant the amount of BDAC and 3BA. Scheme 1 illustrates the synthesis of Au nanoparticles mediated by 3BA.

2.4 Purification of AuNTPs and AuNOC

As mentioned in the introduction, surfactant micelle depletion-induced flocculation was applied for the separation of gold nanoparticles by using CTAC as surfactant. Taking into accoun that the temperature of the syntesis will affect the final particle size (see below), different CTAC concentrations were used in each case. We describe in this section the separation procedure for particles prepared at 1.5 mM $HAuCl_4$ and at 75°C, 85°C and 95°C.

Synthesis at 75°C. Initially, in order to remove the bigger particles generated during the Au synthesis, the colloidal dispersion was centrifuged at 7500 rpm during 30 min. The supernatanat was discarded and the precipitate was redispersed in a 5 mL vial containing 2 mL of CTAC 100 mM. After 4 h at RT, a precipitate (containing bigger particles) was observed at the bottom of the vial, which was discarded (Scheme 1 separation 1). The supernatant, containing a mixture of prisms and octahedra, was again centrifuged at 7500 rpm during 30 min. The supernatant was discarded and the precipitate was redispersed in a 5 mL vial

containing 2 mL of 175 mM CTAC. After 4 h the supernatant, containing AuNOC, was separated, and the precipitate formed at the bottom of the vial, containing AuNTPs, was redispersed in 10 mL of 100 mM CTAC (Scheme 1, separation 2).

Synthesis at 85°C: The colloidal dispersion obtained at 85°C was centrifuged at 8000 rpm during 30 min. The supernatant was discarded and the precipitate redispersed in2 mL of CTAC 125 mM in order to promote the depletion of the bigger particles. The supernatant was concentrated (8000 rpm, 30 minutes) and redispersed in 2 mL of CTAC 200 mM in order to promote the depletion of AuNTPs while AuNOC will remain in solution.

Synthesis at 95°C: The colloidal dispersion synthesized at 95°C was centrifuged at 8500 rpm during 30 min. The supernatant was discarded and the precipitate redispersed in 2 mL of CTAC 200 mM in order to promote the depletion of the bigger particles. The supernatant was concentrated (8500 rpm, 30 minutes) and redispersed in 2 mL of CTAC 250 mM in order to promote the depletion of AuNTPs while AuNOC will remain in solution.

2.5 Synthesis of Au@pNIPAM and Au overgrowth

To carry out the encapsulation of gold prisms and octahedra within pNIPAM microgels, firstly, 10 mL of each Au colloidal dispersion ([Au]≈ 5 mM) obtained after purification step was heated at 70°C under N_2 flow. Then *N*-isopropylacrylamide (0.1698 g, 100 mM) and *N,N'*-methylenebisacrylamide (0.0234 g, 10 mM) were added under magnetic stirring. After 15 min, the N_2 flow was removed and the polymerization was initiated by adding 2,2'-azobis(2-methylpropionamidine) dihydrochloride (10 µL 0.1 M in water). After 2 h at 70°C, the turbid mixture was allowed to cool down to room temperature under stirring. Finally, to remove small oligomers, unreacted monomers as well as gold-free microgels, the dispersion was diluted with water (50 mL) and centrifuged (30 min at 5500 rpm), the resulting pellet was redispersed in water. This process was repeated 3 times.

The AuSTs@pNIPAM particles were obtained by following the same overgrowth procedure previously reported by Liz-Marzan et al.[34] To a 10 mL growth solution containing 0.5 mM $HAuCl_4$, 8 mM CTAB and 4 mM ascorbic acid 0.5 mL of AuNTP@pNIPAM seed solution (1 mM in terms of gold) were added.
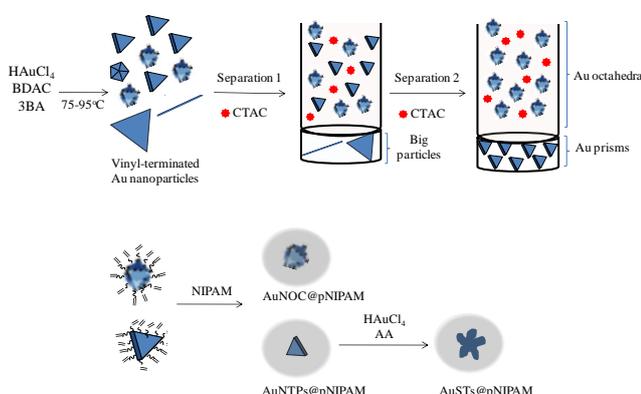
Scheme 1. General procedure for the synthesis of vinyl-terminated gold nanoparticles and shape-separation by surfactant micelle induced depletion interaction. (top) Core@shell Au@pNIPAM fabrication and gold overgrowth (bottom).

3. Results and Discussion

3.1 Synthesis and characterization of Au nanoparticles

As mentioned in the introduction, only few methods has been reported concerning the synthesis of gold nanoparticles with either triangular or octahedral morphologies in aqueous media. In addition, such synthesis procedures do not confer any surface functionality to the as prepared nanoparticles. In order to develop a one-step functionalization, and a highly reproducible methodology using $HAuCl_4$ as gold source, we used 3BA in presence of BDAC as stabilizer. It should be noted that initially we used CTAC as stabilizer, as in the previous mentioned methods. Unfortunately, highly polydisperse gold nanoparticles morphologies together with undefined morphologies were obtained (Fig S1, Supporting Information, SI). Then, we replace CTAC for BDAC, a surfactant with a similar structure, which contains a benzyl group instead a methyl group in its structure. Initially, we analyzed the influence of the gold salt concentration and the temperature in the size and shape of gold nanoparticles (see Table 1).

First, we analyzed the effect of the gold salt precursor at a given temperature; initially, a precursor solution (see experimental section) was heated to 75°C leading to a great number of well-defined AuNTPs (yield 58%) and AuNOC (yield 37%) (see Fig 1A), along with a small number of decahedra and bigger particles (yield 4% and 1%, respectively). The average side length, determined by TEM analysis, was 54.8 ± 4.0 nm and 35.2 ± 2.5 nm for AuNTPs and AuNOC, respectively. Increasing the gold salt concentration to 1 mM leads also to AuNTPs and AuNOC nanoparticles (see Fig 1B) with percentages of 46% and 36 %, respectively (Table 1). Interestingly, a higher percentage (10%) of relatively big particles was also observed. The average dimension of the particles increases 65.8 ± 3.9 nm and 41.9 ± 2.7 nm for AuNTPs and AuNOC, respectively (Table 1, Fig S2). A similar trend was observed when the synthesis was performed with 1.5 mM $HAuCl_4$ (Fig 1C), that is, the percentage of AuNTPs, AuNOC, decahedra and bigger particles decreased to 40%, 30%, 9% and 20%, respectively. On the other hand, the average side lengths for AuNTPs and AuNOC increased to 74.7 ± 5.6 nm and 47.5 ± 3.9 nm, respectively.

Fig 1F shows the normalized UV-vis spectrum of the as prepared aqueous dispersion of gold nanoparticles synthetized at 75°C in the presence of 0.5 mM, 1.0 mM and 1.5 mM $HAuCl_4$. A clear red-shift in the position of the localized surface plasmon resonance from 569 to 583 nm is observed, which is produced by the increase in the average particle size.[45] The UV-vis spectra also show a broad shoulder located at longer wavelengths (700-800 nm) for 1.0 and 1.5 mM $HAuCl_4$, which can be ascribed to the presence of bigger particles. The intensity of the shoulder increases with the gold salt concentration in the reaction mixture, suggesting an increase in the percentage of bigger particles as confirmed by TEM analysis.

T
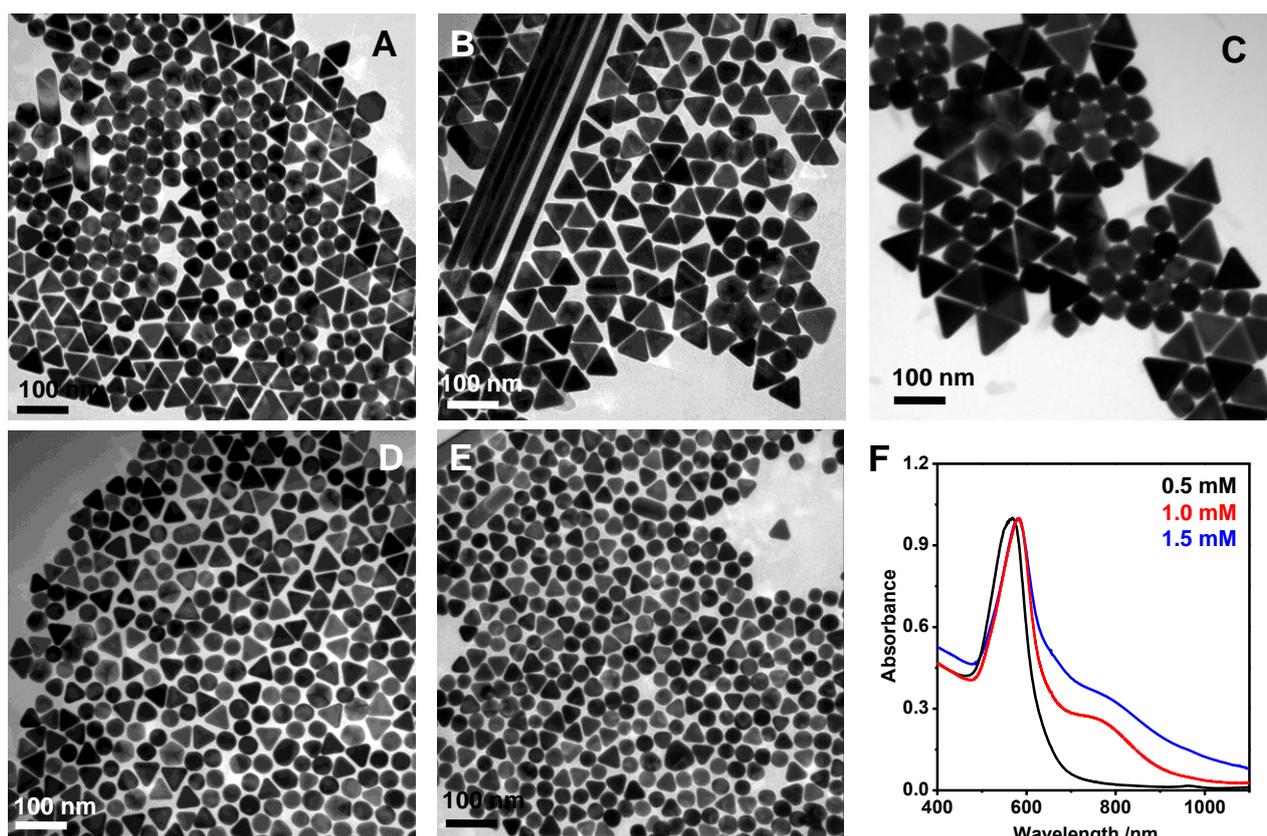
Fig. 1. TEM images of the gold nanoparticles synthesized at 75°C under different concentration of HAuCl$_4$ A) 0.5 mM, B) 1.0 mM and C) 1.5 mM. D) 0.5mM, 85°C E) 0.5 mM, 95°C F) UV-vis spectra of the three colloidal solution synthesized at 75°C at 0.5 (black line), 1.0 (red line) and 1.5 mM HAuCl$_4$ (blue line)

We also studied the influence of the temperature on the size and shape of the particles at a given gold salt concentration. We have chosen 0.5 mM HAuCl$_4$ since gave rise to the lowest contamination of bigger particles. Overall, well-dispersed AuNTPs and AuNOC morphologies where found in all studied cases. At 85°C, the average side length of AuNTPs and AuNOC was 44.9 ± 3.7 and 34.6 ± 2.7 nm, respectively (see Fig S4, SI). When the reaction temperature was raised up to 95°C, the average side length size decreased to 33.3 ± 3.0 nm and 26.6 ± 2.0 nm for AuNTPs and AuNOC, respectively. Fig 1D and 1E show TEM images of the gold nanoparticles synthesized at 85°C and 95°C, respectively. This tendency suggests that an increase in the reaction temperature led to a higher nucleation rate leading to smaller particles. Concerning the influence of temperature on the relative populations of AuNTPs and AuNOC, it should be noted that the percentage of AuNTPs decreased from 58% to 50% when the temperature was increased from 75°C to 95°C. On the other hand, the percentage of AuNOC increased from 37% to 46% (see Table 1).

We also studied the influence of the temperature in the overall reaction rate. It is well-known that temperature is a key parameter in the synthesis of metal nanoparticles since it can greatly modified the nucleation and growth steps. We have measured the time evolution UV-vis spectra for the reaction at 75°C, 85°C and 95°C in the presence of 0.5 mM HAuCl$_4$, see Fig 2. At the beginning only a

Table 1. Size of the AuNTPs and AuNOC synthesized at three different concentration of HAuCl$_4$ at 75°C (reaction times are also included). Percentage of triangular prisms, octahedra, decahedra and bigger particles obtained at 75, 85 and 95°C at 0.5 mM of HAuCl$_4$.

	75 ºC						85 ºC		95 ºC	
[HAuCl$_4$]	0.5 mM		1.0 mM		1.5 mM		0.5 mM		0.5 mM	
Time / min	23						15		7	
	nm	%	nm	%	nm	%	nm	%	nm	%
AuNTPs	54.8	58	65.8	46	74.7	41	44.9	55	33.3	50
AuNOC	35.2	37	41.9	36	47.5	30	34.6	41	26.6	46
Decahedra		4		8		9		3		2
Big Particles		1		10		20		1		2

band located at ca. 325 nm that corresponds to the Au^{3+} is observed (black spectra in Fig 2), upon addition of 3BA this band decreases due to the progressive reduction to Au$^+$. Followed by the appearance of a new band around 500-600 nm, ascribed to the nucleation of gold nanoparticles. Subsequently, the band increases in intensity and becomes sharper and better defined due to the growth of the particles (Fig 2A-C). Figure 2D represents the increase of the absorbance at 400 nm with time at the three mentioned temperatures. The difference in the reaction rate can be easily
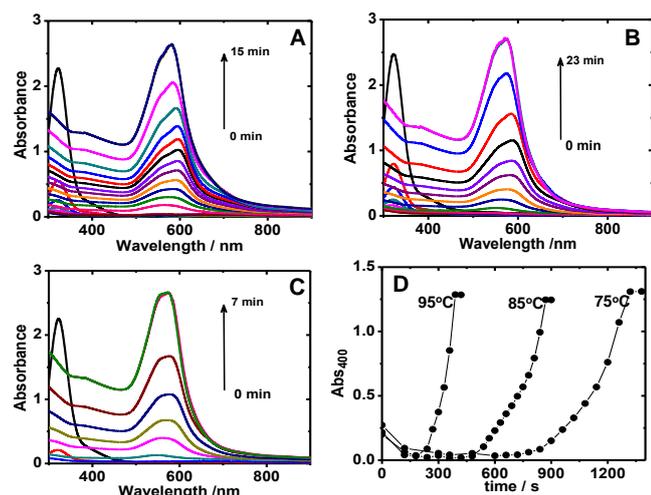
Fig 2. UV-vis spectral evolution for the synthesis performed at 0.5 mM of $HAuCl_4$ at A) 75°C, B) 85°C and C) 95°C. Evolution of the absorbance at 400 nm for the three mentioned temperatures D).

observed; while at 75°C the absorbance reached a maximum at 23 min, when the synthesis was performed at 85°C and 95°C the time need to reach the maximum absorbance decreased to 15 min and 7 min, respectively. It should be noted that in all cases the final UV-vis spectra showed a narrow localized surface plasmon band, suggesting the absence of bigger particles.
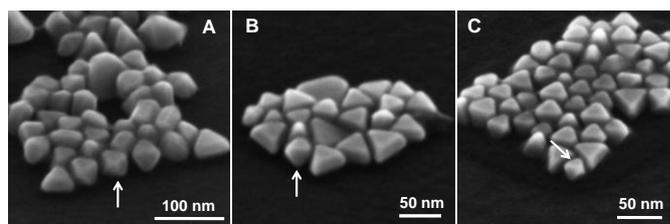
Fig 3. Tilted FESEM images of the Au nanoprismsAuNOCsynthesized at 0.5 mM of $HAuCl_4$; A) 75°C, B) 85°C and C) 95°C. The white arrows show AuNOCs particles with different orientations.

In order to completely characterize the morphology of the obtained particles, they have been analyzed by FESEM. Figure 3 shows representative tilted FESEM images were the morphologies of AuNTPs and AuNOC nanoparticles can be clearly discerned. Additionally, a detailed study of the AuNTPs dimensions showed a slight decrease in particle thickness as a function of the temperature. The average thickness dimension decreased from 16.6 nm at 75°C to 13.8 nm at 85°C and 9.9 nm at 95°C.

Finally, in order to demonstrate the reproducibility of this procedure, the synthesis procedure performed at 75°C (0.5 mM $HAuCl_4$) was scale up to 250 mL, giving rise to similar results in size, reaction rate and percentage of the main morphologies (Fig. S5, SI).

2.2 Purification of gold nanoparticles

Surfactant micelle induced depletion interaction has been previously reported for the separation of metal nanoparticles
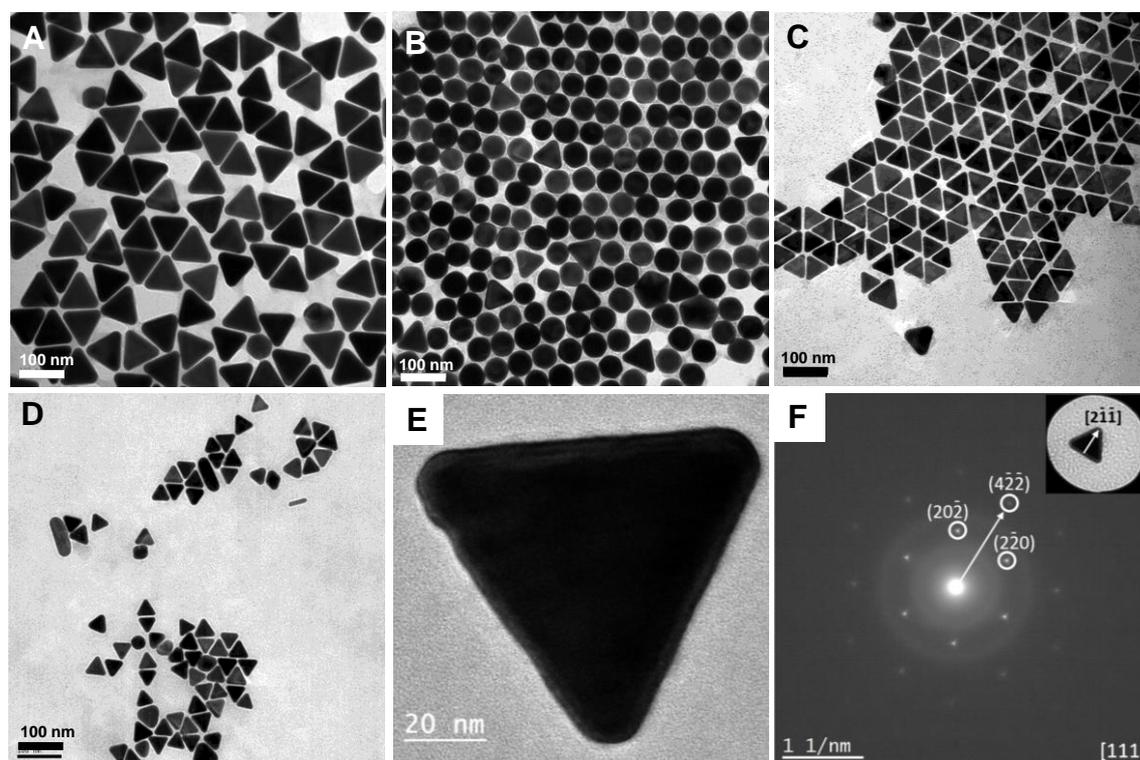
Fig. 4. A) and B) TEM image for the AuNTPs and AuNOC (75°C and 1.5 mM $HAuCl_4$) after depletion-induced flocculation, respectively C) and D) TEM images of the Au NTPs (1.5 mM $HAuCl_4$) after purification step synthesized at 85°C and 95°C, respectively. E) Top view and cross section (inset) of aAuNTP showing flat top and bottom facets. The scale in the inset is 20 nm. F) Selected area electron diffraction pattern obtained from the AuNTP, in the inset we show the prism with the in plane rotation compensated.
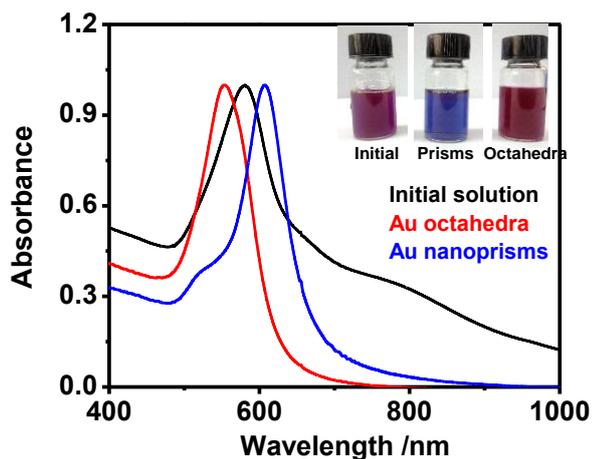
Fig. 5. Normalized UV-vis spectra for the Au nanoparticles synthesized at 75°C and 1.5 mMof HAuCl4 before (black line) and after depletion-induced flocculation, which includes AuNOC (red line) and AuNTPs (blue line). The inset shows an image of a vial containing the AuNTPs and AuNOC colloidal solutions

containing different sizes and shapes. This method is based on the depletion interactions between particles in presence of micelles produced by a surfactant.[45] We carried out the separation process for samples prepared with 1.5 mM of HAuCl$_4$ at the three mentioned temperatures. Initially, bigger particles were flocculated with 100 mM CTAC, as it was confirmed by the TEM images and UV-vis spectrum of the redispersed precipitate (Fig. S6, SI). The remaining supernatant, mainly containing AuNTPs and AuNOC, was subjected to the same separation procedure but with 175 mM CTAC. After this second depletion process the precipitate contained mainly AuNTPs (see Fig 4A) while the supernatant contained AuNOC (see Fig 4B). As it can be clearly observed the percentage of either prisms or octahedra remarkably increases compared with the sample before purification steps (see Fig. 1C). Images at lower magnification are shown in Fig. S7, SI. TEM images corresponding to the AuNTPs synthesized at 85°C and 95°C are included in Fig. 4C and 4D, respectively. As is observed, the number of prisms remarkably increases with respect to samples before depletion. The dimension analysis for the obtained Au prisms resulted in an averageside length of 52.3 ± 3.5 nm, and 42.3 ± 3.2 nm for synthesis at 85 and 95°C, respectively, (Fig S8, SI) data not included in table 1. The crystallographic structure of the AuNTPs has also been analyzed by HR-TEM. A representative top view TEM image of an AuNTPs lying flat on the carbon film is presented in Figure 4E. Prisms show an almost perfect triangular shape with rounded tips. The inset shows a cross section of one of the prism exhibiting a thickness of 43 nm and lateral side facets. Selected area electron diffraction (SAED) pattern, included in Figure 4F, displays a regular reciprocal net that corresponds with the [111] zone axis of the gold crystalline structure. In the inset we show an AuNTP with the in plane rotation compensated; from that we have found the [211] type directions as the crystalline directions parallel to the prisms tips.

The purification process was also monitored by UV-vis spectroscopy. Figure 5 represents the normalized UV-vis spectra of the Au colloidal solutions of the samples prepared at 75 °C and 1.5

mM of HAuCl$_4$, before and after depletion induced separation processes. Initially the spectrum exhibits a maximum plasmon band at 583 nm (black line), and the aqueous colloidal solution displayed a purple color, inset in Fig 5. After purification, the normalized UV-vis spectrum of the isolated AuNOC displays a narrow plasmon band at 554 nm (red line) and the aqueous colloidal solution (included in the inset) shows an intense red color. The normalized UV-vis spectrum of the AuNTPs shows a plasmon band at 602 nm (blue line), and the aqueous colloidal solution displayed an intense blue color.

3.3 Synthesis of ofAu@pNIPAM particles. SERS investigations

As it was mentioned, 3BA supplies vinyl-functionalization onto gold nanoparticles surface.[42] It is important to remark that double bond terminated systems are nowadays used for different purposes; for example, double bond terminated specimens have been recently incorporated on H-Si surface by photoactivated hydrosilylation reaction,[46] and vinyl-finctionalized metal nanoparticles have been encapsulated with a pNIPAM, styrene or silica shell. To this aim, the purified samples containing AuNTPs and AuNOC were performed to free radical polymerization in presence of N-isopropylacrylamide and and N,N'-methylenebisacrylamide. Figs 6A and 6B show representative TEM images of the obtained core@shell AuNTPs@pNIPAM and AuNOC@pNIPAM nanocomposites. Both, AuNTPs and AuNOC are homogeneously coated by a pNIPAM shell. After that, in order to increase the number of tips within the microgel, AuNTPs@pNIPAM particles were used as seeds for an Au core overgrowth, under the same conditions previously reported for Au@pNIPAMparticles,[34] resulting AuSTs@pNIPAM nanoparticles (Figure 6C). It should be noted that in this case the initial seeds are
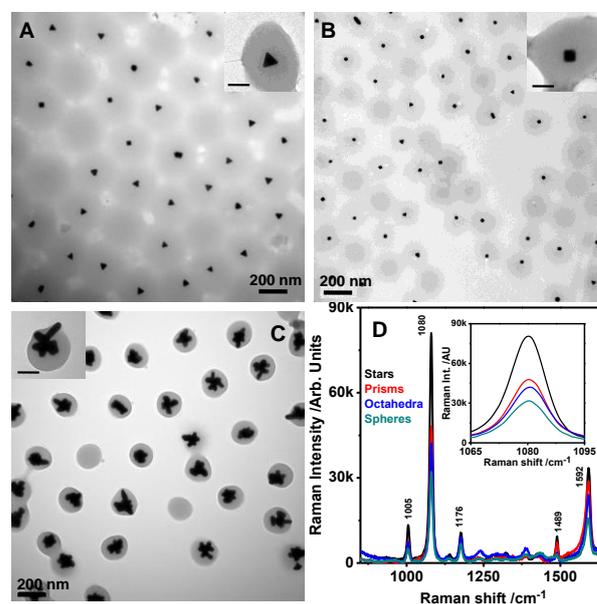
Fig. 6. RepresentaticeTEM images of differentcore@shell hybrid systems. A) AuNTPs@pNIPAM, B) AuNOC@pNIPAM and C) AuSTs@pNIPAM particles. D) Raman spectra of 4ABT (10^{-5} M) aqueous solution adsorbedon the different samples tested. The scale in the inset is 50 nm. The inset in D highlights the Raman shift located at 1080 cm^{-1}.

formed by AuNTPs@pNIPAM, the resulting gold cores in AuSTs@pNIPAM system contains higher number and sharper tips, compared with gold nanostars grown from Au spheres.[34]

SERS investigations were performed by using 4-aminobenzenethiol (4ABT) as model analyte. Figure 6D includes the 785 nm SERS spectra of $1.0x10^{-5}$M 4ABT for the three different samples. In all specimens the Raman peaks corresponding to the 4ABT were clearly observed,[47] including the peaks at 1592 (CC stretching), 1489 (CC stretching + CH bending), 1225, 1176 and 1135 (CH bending), 1080 (CS stretching), 1005 (CC + CCC bending), 822 and 702 (CH, CS and CC wagging) and 636 cm-1 (CCC bending). As expected the SERS intensity increases with the number of tips presented in the metal core. The inset represents the SERS spectra of 4ABT in the spectral range between 1000-1200 cm^{-1}, the intensities of the 4ABT signal follows the expected tendency AuSTs@pNIPAM > AuNTPs@pNIPAM > AuNOC@pNIPAM.

4. Conclusions

We have presented a novel, easy and reproducible seedless method for the synthesis of vinyl-terminated Au nanoparticles in water media by using 3-butenoic acid as reducing agent and BDAC as stabilizer. This method produces triangular prisms and octahedra as principal morphologies. The reaction rate was monitored by UV-vis evolution at three different temperature (75, 85 and 95°C). UV-vis measurements demonstrated that the reaction rate particle is higher when the temperature of synthesis is increased. TEM analysis confirmed that both the average side length of the particles and the amount of big morphologies increase with the concentration of $HAuCl_4$. On contrary, the particle size and the percentage of Au prisms decrease with the temperature. FESEM analysis showed 3D images which confirmed that the particle thickness of AuNTPs also decreased with the temperature. Surfactant micelle induced depletion interaction was used as purification step. This method was able to separate the different morphologies and increased the percentage of Au prisms and octahedra up to ~90%. The vinyl-terminated Au prisms and octahedra were easily encapsulated within a pNIPAM microgel by free radical polymerization, obtaining a hybrid Au@pNIPAM system. The number of tips within the microgel was increased by gold overgrowth under controlled conditions, resulting in an AuSTs@pNIPAM system. SERS investigations demonstrated that Au@pNIPAM particles containing more number of high curvature sites provided improved SERS responses. The method proposed is the first reported procedure for the synthesis of Au nanoprisms and octahedra which enable a direct incorporation of a pNIPAM shell.

Acknowledgements

Notes and references

1 X. C. Jiang, M. P. Pileni, *Colloids and Surf. A: Phys. Eng. Asp.* 2007, **295,** 228.
2   X. H. Huang, P. K. Jain, M. A. El-Sayed, *Nanomedicine* 2007, **2,** 681.
3 S. E. Skrabalak, L. Au, X. Lu, X. Li, Y. Xia, Y. *Nanomedicine* 2007, **2,** 657.
4 S. R. Sershen, S. L. Westcott, N. J. Halas, J. L. West, *J. Biomed. Mater. Res*. 2000, **51,** 293.
5 S. J. Park, C. A. Taton, C. A. Mirkin, *Science* 2002, **295,** 1503.
6 J. J. Storhoff, A. D. Lucas, V. Garimella, Y. P. Bao, U. R. Muller,. *Nat. Biotechnol.* 2004, **22,** 883.
7 N. T. K. Thanh, Z. Rosenzweig, *Anal. Chem*. 2002, **74,** 1624.
8 I. H. El-Sayed, X. H. Huang, M. A. El-Sayed,. *Nano Lett*. 2005, **5,** 829.
9 S. Lal, S. E. Clare, N. J. Halas, *Acc. Chem. Res.* 2008, **41,** 1842.
10 J. Chen, D. Wang; J. Xi, L. Au, A. R. Siekkinen, A. Warsen, Z.–Y. Li, H. Zhang, Y. Xia, X. Li, *Nano Lett.* 2007, **7,** 1318.
11 D. Astruc, F. Lu, J. R. Aranzaes, *Anweg. Chem. Int. Ed.* 2005, **44,** 7852.
12 M. Daté, M. Okumura, S. Tsubota, M. Haruta, *Angew. Chem. Int. Ed.* 2004, *43,* 2129.
13 U. Kreibig, M. Vollmer,. Optical Properties of Metal Clusters; Springer: Berlin, Germany, 1995.
14 S. Link, M. A. El-Sayed, *Int. Rev. Phys. Chem.* 2000, **19,** 409.
15 J. Rodríguez-Fernández, J. Pérez-Juste, F. J. García de Abajo, L. M. Liz-Marzán, *Langmuir* 2006, **22,** 7007.
16 J. Turkevich, P. C. Stevenson, J. Hillier, *J. Phys. Chem.* 1953, **57,** 670.
17 I. Pastoriza-Santos, L. M. Liz-Marzan,. *J. Mater. Chem.* 2008, **18,** 1724.
18 C. Xue, G. S. Metraux, J. E. Millstone, C. A. Mirkin, *J. Am. Chem. Soc.* 2008, **130,** 8337.
19 B. Nikoobakht, M. A. El-Sayed, *Chem. Mater.* 2003, **15,** 1957.
20 X. M. Lu, M. S. Yavuz, H. Y. Tuan, B. A. Korgel, Y. N. Xia, *J. Am. Chem. Soc.* 2008, **130,** 8900.
21 W. Li, Y. Xia, *Chem Asian J.* 2010, **5,** 1312.
22 A. Sánchez-Iglesias, I. Pastoriza-Santos, J. Pérez-Juste, B. Rodríguez-González, F. J. García de Abajo, L. M. Liz-Marzán, *Adv. Mater*. 2006, **18,** 2529.
23 L. Polavarapu, S. Mourdikoudis, I. Pastoriza-Santos, J. Pérez-Juste, *Cryst Eng Comm.* 2015, **17,** 3727.
24 M. Grzelczak, J. Perez-Juste, P. Mulvaney, L. M. Liz-Marzan. *Chem. Soc. Rev.* 2008, **37,** 1783.
25 F. Kim, S. Connor, H. Song, T. Kuykendall, P. Yang, *Angew. Chem. Int. Ed.* 2004, **43,** 3673.
26 C. Li, K. L. Shuford, M. Chen, E. J. Lee, O. S. A. Cho, *ACS Nano* 2008, **2,** 1760.
27 M. R. Langille, M. M. L. Personick, J. Zhang, C. A. Mirking. *J. Am. Chem. Soc.* 2011, **133,** 10414-14417. .
28 J. Xie, J. Y. Lee, D. I. C. Wang, *Chem. Mater.* 2007, **19,** 2823-2830.
29 W. Niu, S. Zheng, D. Wang, X. Liu, H. Li, S. Han, J. Chen, Z. Tang, G. Xu, *J. Am. Chem. Soc.* 2009, **131,** 697.
30 D. Seo, J. C. Park, H. Song, *J. Am. Chem. Soc.* 2006, **128,** 14863.
31 N. R. Jana, L. Gearheart, C. J. Murphy, C. J. *Adv. Mater*. 2001, **13,** 1389.
32 L. Scarabelli, M. Coronado-Puchau, J. J. Giner-Casares, J. Langer, L. M. Liz-Marzán, *ACS Nano* 2014, **8,** 5833.
33 L. Chen, F. Ji, Y. Xu, L. He, Y. Mi, F. Bao, B. Sun, X. Zhang, Q. Zhang, *Nano Lett.* **2014,** *14,* 7201.

Nanoscale Accepted Manuscript

34 R. Contreras-Caceres, A. Sanchez-Iglesias, M. Karg, I. Pastoriza-Santos, J. Perez-Juste, J. Pacifico, T. Hellweg, A. Fernandez-Barbero, L. M. Liz-Marzan, *Adv. Mater.* 2008, **20,** 1666.

35 Y. Lu, Y. Mei, M. Drechsler, M. Ballauff, *Angew. Chem. Int. Ed.*2006,**45,** 813.

36 R. Contreras-Caceres, S. Abalde-Cela, P. Guardia-Giros, A. Fernandez-Barbero, J. Perez-Juste, R. A. Alvarez-Puebla, L. M. Liz-Marzan, *Langmuir* 2011,**27,** 4520.

37 M. Laurenti, P. Guardia, R. Contreras-Caceres, J Perez-Juste, A. Fernandez-Barbero, E. Lopez-Cabarcos, J. Rubio-Retama, *Langmuir* 2011**,** *27,* 10484.

38 R. A. Alvarez-Puebla, R. Contreras-Caceres, I. Pastoriza-Santos, J. Perez-Juste, L. M. Liz-Marzan, *Angew. Chem. Int. Ed.*2009, **48,** 138.

39 L. Zha, Y. Zhang, W. Yang, S. Fu, *Adv. Mater.*2002, **14,** 1090.

40 J. –H. Kim, T. R. Lee, *Chem. Mater.* 2004, **16,** 3647.

41 J. –H. Kim, T. R. Lee, *Langmuir* 2007, **23,** 6504.

42 R. Contreras-Caceres, I. Pastoriza-Santos, R. A. Alvarez-Puebla, J. Perez-Juste, A. Fernandez-Barbero, L. M. Liz-Marzan. *Chem. Eur. J.* 2010, **16,** 9462.

43 S. Gómez-Graña, C. Fernández-López, L.Polavarapu, J. Baptiste Salmon, J. Leng, I. Pastoriza-Santos, J. Pérez-Juste, *Chem. Mater.* 2015, **27**, 8310.

44 K. Park, H. Koerner, R. A. Vaia, *Nano Lett.* 2010, **10,** 1433.

45 N. R. Jana, *Chem. Commun.* 2003, 1950.

46 A. Lucena-Serrano, C. Lucena-Serrano, R. Contreras-Caceres, A. Diaz, M. Valpuesta, C. Cai, J. M. Lopez-Romero. *Appl. Surf. Sci*. 2016, **360,** 419.

47 K. Kim, J.-Y. Choi, H. B. Lee, K. S. Shin. *J. Chem. Phys*. 2011, **135,** 124705.